Discover Applied Sciences

Research

Exploring the chemical properties and microstructural characterisations of hybrid asphalt binders for enhanced performance

Wan Noor Hin Mior Sani[1] · Ramadhansyah Putra Jaya[1] · Khairil Azman Masri[1] · Kushendarsyah Saptaji[2] · Anmar Dulaimi[3,4]

Received: 6 February 2024 / Accepted: 27 March 2024
Published online: 05 April 2024

Abstract
Approximately 3 billion metric tonnes of garbage involving industrial and agricultural waste is expected to be generated by 2030, posing a significant environmental hazard. Notably, recycling or reusing asphalt modification components (palm oil fuel ash (POFA), garnet waste, and sawdust) in pavement construction encounter ongoing challenges. This study comprehensively assessed the chemical characteristics and microstructure analysis of individual wastes and various hybrid asphalt binder and mixtures incorporated with these components. The mixture consisted of asphalt grade 60/70 blended with varying amounts (0%, 3%, 6%, and 9%) of POFA, garnet waste, and sawdust. Fourier transform infrared spectroscopy (FTIR), X-ray fluorescence (XRF), and X-ray diffraction (XRD) analyses were also employed to examine the chemical compositions of the raw waste materials. Meanwhile, the microstructure properties of various hybrid asphalt binder mixtures were analysed utilising Scanning Electron Microscopy (SEM) and Atomic Force Microscopy (AFM). Consequently, this study presented that the correlation between the 6% POFA, 6% garnet waste, and 6% sawdust substantially impacted the chemical composition and morphology of the mixture. The findings of this study demonstrated that including POFA, garnet waste, and sawdust in a hybrid asphalt binder and mixture could enhance performance and engineering properties.

Article Highlights

- XRD, XRF, FTIR, SEM, and AFM identified chemical properties and morphology characterisation.
- The study examines the correlation between raw materials properties; POFA, garnet waste and sawdust with hybrid asphalt mixture as a combination of the three wastes.

Keywords Hybrid asphalt · Palm oil fuel ash · Garnet waste · Sawdust · Chemical properties · Microstructure · Scanning electron microscopy · Atomic force microscopy

✉ Ramadhansyah Putra Jaya, ramadhansyah@umpsa.edu.my | [1]Faculty of Civil Engineering Technology, Universiti Malaysia Pahang Al-Sultan Abdullah, 26300 Kuantan, Pahang, Malaysia. [2]Department of Mechanical Engineering, Faculty of Engineering and Technology, Sampoerna University, Jakarta 12780, Indonesia. [3]College of Engineering, University of Kerbala, Karbala 56001, Iraq. [4]College of Engineering, University of Warith Al-Anbiyaa, Karbala 56001, Iraq.

1 Introduction

The utilisation of industrial and agricultural waste materials to enhance the sustainability of bitumen modification is vital. Notably, palm oil fuel ash (POFA) is a residual substance derived from the palm oil industry, which demonstrates excellent potential as a viable option for improving bitumen characteristics [1–3] . This material can address the environmental difficulties of waste disposal while creating a more robust and environmentally friendly infrastructure. Similarly, garnet waste (a by-product of the gemstone industry) and sawdust (a by-product of agricultural activities) extend the possibilities of sustainable bitumen modification [4]. Hence, the correlation examination between these waste components and bitumen is crucial for discovering inventive solutions to produce durable and environmentally aware road pavements [5, 6].

Although bitumen modification involves adjusting the composition, the process also profoundly impacts the chemical and microstructural features of the resulting asphalt. When the molecular dynamics and microscale interactions are investigated, the transformative impact of modification on the fundamental characteristics of bitumen can be understood. Numerous characterisation tools are also essential for studying changes at the chemical and microstructural levels, including Scanning Electron Microscopy (SEM), Atomic Force Microscopy (AFM), X-Ray Fluorescence (XRF), X-Ray Diffraction (XRD), and Fourier Transform Infrared Spectroscopy (FTIR)[7–9]. Therefore, understanding these complex changes can improve the understanding of modified bitumen. This process also establishes a basis for customising the characteristics to satisfy the rigorous requirements of sustainable and high-performance road construction [10–12].

Multiple studies have investigated using POFA, garnet waste, and sawdust in bitumen modification, mainly relying on advanced chemical testing methodologies [13–15]. The XRD and XRF analyses have demonstrated a crucial role in understanding the crystalline structure changes and elemental composition caused by POFA in the bituminous matrix. POFA primarily comprises SiO_2 alongside K_2O, MgO, CaO, and traces of Al_2O_3 [13, 16, 17]. A study by Alnahhal et al. used XRD to verify the potential use of POFA as a partial substitute in lightweight concretes [18]. The study highlighted that the highest chemical composition was 50% SiO_2, followed by 6.70% Fe_2O_3 and 2.07% Al_2O_3. Meanwhile, the FTIR analysis of the POFA-modified bitumen revealed distinct peaks corresponding to the functional groups in the ash. This outcome denoted the successful chemical bonding between the two materials [19]. Likewise, a study by Mulizar et al. [20] documented that the FTIR analysis presented stretching in the Si–O–Al gel of the POFA material.

A study by Muttashar et al. [21] applied XRD to determine that garnet waste comprised a significant proportion of Fe_2O_3, SiO_2, and Al_2O_3. Alternatively, Aletba et al. [14] further examined the chemical composition of garnet waste as an aggregate substitute in asphalt mixtures. The study emphasised that the chemical composition generated elevated Fe_2O_3 and SiO_2 levels. Another study by Usman et al. [22] conducted a laboratory assessment to illustrate that the rigidity of cold mix asphalt was significantly impacted by the chemical composition using XRF and XRD (irrespective of the specific asphalt binder employed). The validity of the study was reinforced by the significant Fe_2O_3 content in manually and automatically generated waste spent garnet. This outcome was demonstrated by the XRF analysis and the presence of quartz in manually and automatically generated waste spent garnets. The FTIR result offered an additional avenue of investigation regarding the XRD result [19]. A study by Muttashar et al. [23] recorded that FTIR analysis of garnet waste incorporation revealed shifts in specific spectral bands. This finding indicated that the chemical interactions enhanced the overall cohesiveness of the modified bitumen. The FTIR spectra of the spent garnet also illustrated that the bonding vibrations of OH and Si–O groups caused the absorption bands. Thus, the existence of these groups frequently exerted a notable influence on the rate at which water was absorbed and the process of differentiating mineral composition.

The introduction of sawdust causes noticeable alterations in the broadening of XRD peaks, suggesting crystalline nature changes in the bitumen. Sawdust ash is a low-density substance composed of Ca, Si, Al, Fe, S, K, Mg, W, and P oxides [35, 36]. This material acquires a specific gravity of 2.29 [15]. Specifically, CaO is the highest chemical component observed, indicating a strong bond between the asphalt binder and the aggregate. This compound improves the bonding and cohesiveness of asphalt modification. Hence, integrating sawdust resulted in elemental composition changes (characterised by increased C content), contributing to enhanced tensile strength in XRF. Another two studies by Karati and Roy and Ing et al. utilised XRF to evaluate and quantify the proportion of the present element in sawdust ash, leading to high CaO amounts [24, 25]. This outcome could enhance the CaO interaction with the asphalt binder. Other studies by Osuya and Mohammed and Wang et al. applied XRF to measure the chemical constituents of sawdust ash, which confirmed insufficient presence of CaO components [26, 27]. This finding ensured that no

risk of environmental pollution was indicated. Likewise, a study by Couto et al. investigated the FTIR spectrum of sawdust. The study exhibited a broad band at approximately 3400 cm^{-1}, corresponding to the axial OH deformation [28]. Additionally, signals at 2930 cm^{-1} indicated the symmetric and asymmetric vibrations of $–CH_2–$ groups. Another study by Ayuba conducted an SEM analysis on ash particles from different sources [29]. The study observed variations in physical characteristics (particle size and shape), which were influenced by the incineration method. In addition, the study discovered that sawdust ash (SDA) acquired high CaO and SiO_2 levels, which increased ignition loss due to uncontrolled incineration.

Three prominent findings became apparent upon analysing previous studies. Firstly, the SEM scans demonstrated a more even distribution of POFA particles inside the bituminous matrix, improving the overall stability. These SEM studies also reported that the POFA particle exhibited a rough surface, resulting in decreased workability and an extended setting time compared to the 5% POFA-based mixture [20]. The ground POFA generally displays irregular, thinner, and crushed particles arranged in clusters of spherical particles with minimal air space between them [30]. A study by Usman et al. provided the micrograph results of the garnet waste samples at a 25% level using SEM, which reduced particle accumulation [31]. The study provided the micrograph results of the garnet waste samples at a 25% level, which reduced particle accumulation. Consequently, a distinct gel-like substance was developed based on the SEM analysis and corroborated by its reduced strength. Overall, POFA is a raw material characterised by highly asymmetrical particle morphologies and porous cellular surfaces [32].

The second finding of the previous studies involved garnet waste addition for a well-defined microstructural arrangement. This process enhanced the bonding capabilities of the material. The garnet waste related SEM images generated a modified surface morphology, interlocking particles and forming a denser matrix. A study by Ibrahim et al. documented several well-defined structures of the garner with sharp edges [33]. This design allowed for multiple contact areas with excellent tensile strength, and the material could be cut with rigidity. Likewise, a study by Yuan et al. [34] employed tapping mode in AFM at room temperature to determine that ageing led to a lower bonding force in the catana, peri, and para phases. Another study by Garcia et al. utilised contact and pulse force modes and discovered that bonding and stiffness increased with ageing [35]. Finally, these previous studies showcased that AFM investigations presented the complex interlocking of sawdust with bitumen, resulting in improved tensile strength. Highly rigid cellulose crystals revealing a stick-like form in the SEM micrographs of sawdust ash were also noticed, which varied in length and width [36]. Thus, the data obtained from the morphological analyses of AFM verified the high efficiency of utilising ultrasonic techniques to accelerate the acid hydrolysis of sawdust waste for cellulose nanocrystal production.

This study thoroughly investigated the performance of bitumen modification, considering the issues presented by deteriorating road pavements and the increasing importance of sustainable infrastructure. Novel approaches for improving the chemical and morphological characteristics of bitumen were also explored by carefully integrating three specific waste materials: POFA, garnet waste, and sawdust. Therefore, the distinctive combination of these waste elements offered the potential to address waste disposal-related environmental issues and transform the current asphalt engineering practices. This study provided valuable insights into the chemical complexities and microstructural intricacy of asphalt modified with POFA, garnet waste, and sawdust. The outcome of this study could promote more sustainable, robust, and environmentally conscious road construction practices.

Table 1 Summary of the basic properties of the 60/70 PEN asphalt

Parameter	Specification	Result	Requirement
Penetration (25 °C, dmm)	ASTM D5	70	60–70
Softening point (°C)	ASTM D36	47.6	49–56
Ductility (25 °C, Pa s)	ASTM D113	100	≥ 100
Viscosity (135 °C, Pa s)	ASTM D4402	0.5	< 3

ASTM = American Society and Testing Materials

Table 2 Summary of the physical indicators of the waste materials

Waste material	POFA	Garnet waste	Sawdust
Density (g/cm^3)	2.51	2.96	0.26
Specific gravity	2.51	2.97	1.23
Moisture content (%)	6.10	0.40	5.02

2 Materials and methods

2.1 Materials

This study utilised a 60/70 penetration grade asphalt obtained from the Kemaman Bitumen Company (KBC), Terengganu, Malaysia. Table 1 lists the various engineering characteristics of the initial asphalt using standard empirical methods. The waste materials utilised included POFA, garnet waste, and sawdust. Table 2 illustrates the physical characteristics of the waste materials. This study then applied agricultural (POFA with sawdust) and industrial (garnet) wastes for the hybrid asphalt binder mixtures. All these materials were sieved to achieve a uniform particle size of 25 µm. The POFA was distinguished by its small particle size and dark grey colour. In contrast, the garnet waste presented a reddish-grey hue. Meanwhile, the sawdust was recognised by its light brown colour. Figure 1 depicts the research flowchart, which classifies into three distinct categories: raw materials, waste-modified asphalt binder, and hybrid asphalt binder and mixture.

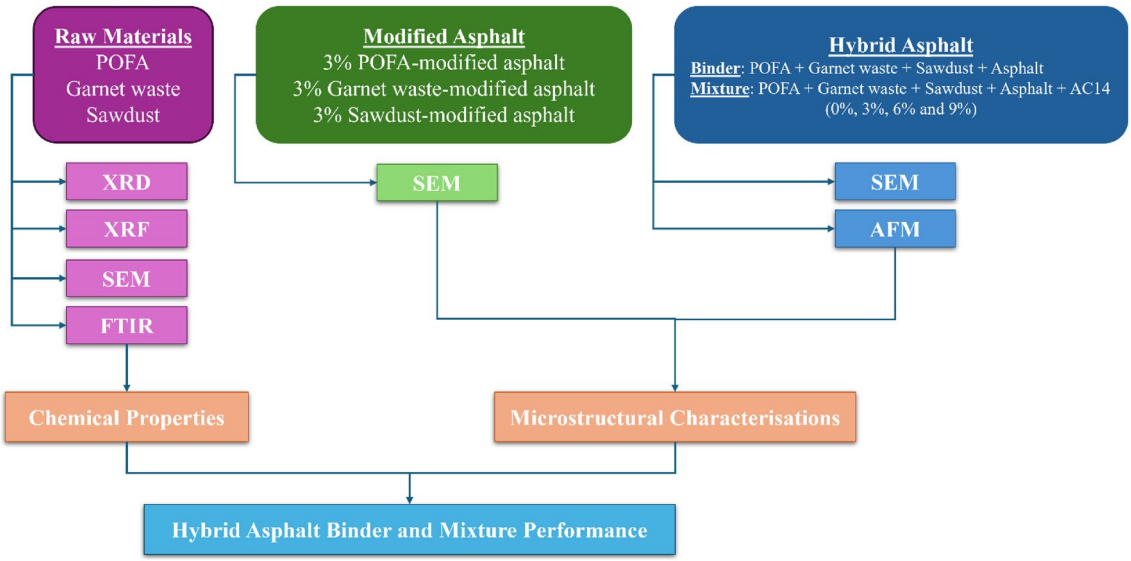

Fig. 1 Flowchart of this research

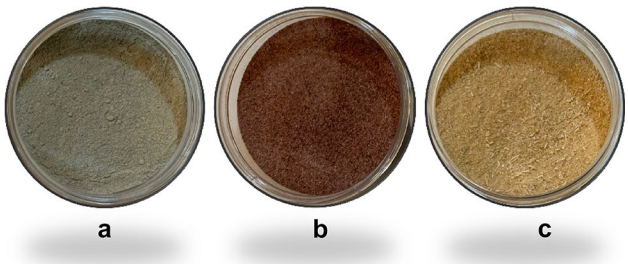

Fig. 2 The waste materials involving **a** POFA, **b** garnet waste, and **c** sawdust

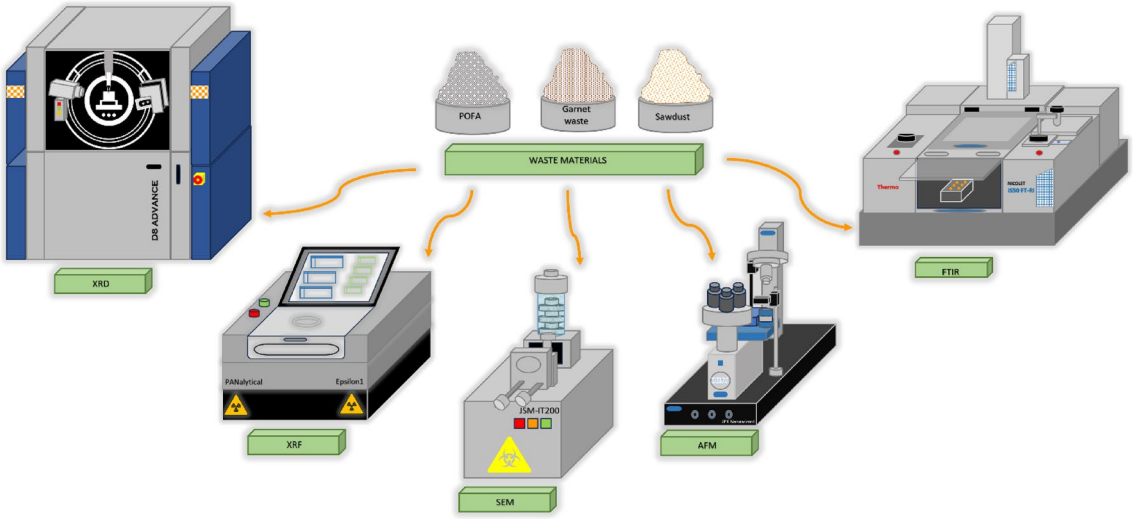

Fig. 3 The chemical test for the composition and properties analyses of the individual wastes

Table 3 Proportion of the materials used and testing involved

Asphalt name	Type	Proportion	Testing
Raw materials	POFA Garnet waste Sawdust	Amount depending on the test in mg	XRD, XRF, SEM, FTIR
Modified asphalt	POFA-modified asphalt Garnet waste-modified asphalt Sawdust-modified asphalt	3%	AFM
Hybrid asphalt binder	POFA + Garnet waste + Sawdust + Asphalt 60/70	0%, 3%, 6%, 9%	SEM, AFM
Hybrid asphalt mixture	POFA + Garnet waste + Sawdust + Asphalt 60/70 + AC14	0%, 3%, 6%, 9%	SEM, AFM

2.2 Preparation of waste materials

The study involved drying POFA, garnet waste, and sawdust at 100°C and then sieving them to a particle size of 25 µm (see Fig. 2). Figure 3 depicts the three distinct waste materials that undergo XRD, XRF, FTIR, SEM, and AFM analyses. Table 3 is the proportion of the materials used and testing involved in this study. Concurrently, the waste materials used in this study were POFA, garnet waste and sawdust; POFA-modified, garnet waste-modified, and sawdust-modified asphalts with a 3% waste content and hybrid asphalt which contain the combination of POFA + garnet waste and sawdust. These materials were then examined using SEM and AFM.

2.2.1 XRD test

The XRD instrument (Bruker D8 Advance Diffractometer) was fitted with a Cu radiation source with a wavelength of 1.54060 Å, which assessed the structural properties of POFA, garnet waste, and sawdust. This instrument was operated using X-pert software with a current of 40 mA and a voltage of 45 kV. Initially, a fraction of each sample was placed in the sample holder of the instrument to characterise the components. The samples were then analysed using a step size of 0.05° and a scanning period of 2 s/data point. Moreover, the scan range encompassed a 2θ angle from 10° to 80°. This scanning technique facilitated the acquisition of diffraction patterns and enabled the examination of the crystallographic structure of the samples.

2.2.2 XRF test

The chemical investigation of the waste materials was conducted using an XRF instrument (Epsilon 1 PANalytical). These samples were prepared into circular pellets using a hydraulic press for 10 s while applying a load of 20 t. Each analysed

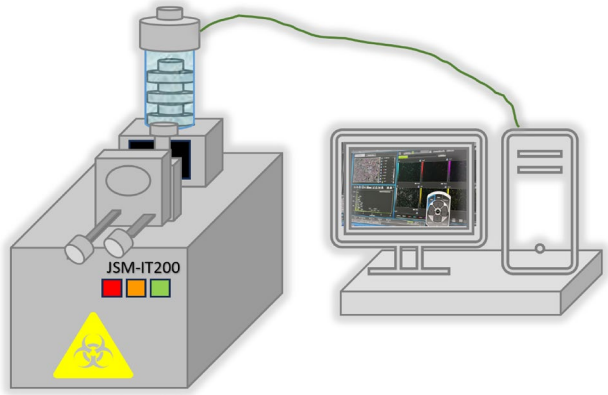

Fig. 4 The SEM test using the JSM-IT200 model

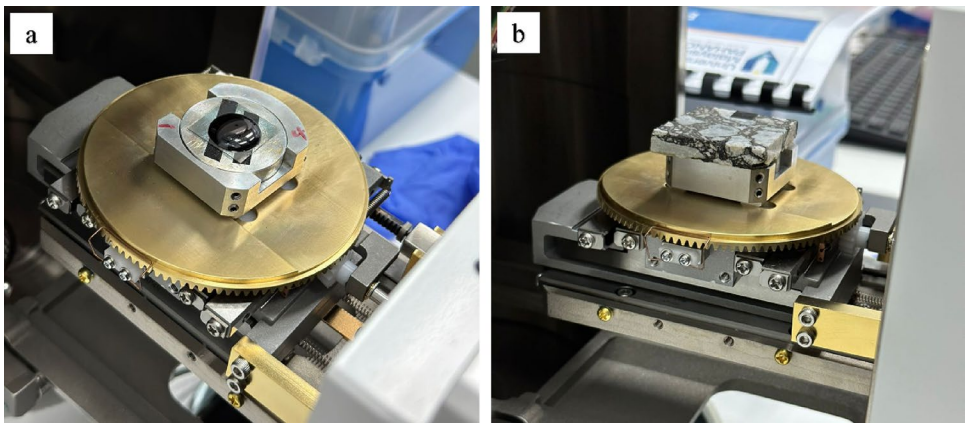

Fig. 5 The placements in the SEM instrument involving the **a** hybrid asphalt binder and the **b** hybrid asphalt mixture

sample comprised 10 g of waste material in the form of dry powder, and the XRF analysis was conducted following the British standard European standard International Organization for Organization (BS EN ISO) 12677 standard. Subsequently, a custom-made X-ray tube with a silver (Ag) anode source (functioning at 50 kV) was used. Lastly, the samples and their corresponding elements were identified based on the unique XRF emitted by the sample when exposed to X-rays.

2.2.3 FTIR test

An FTIR instrument (Thermo Fisher Scientific/Nicolet iS50) was employed to deter-mine the vibrational modes of the POFA, garnet waste, and sawdust. The spectrometer was utilised in absorption mode in the 400–4000 cm^{-1} frequency range. Additionally, the analysis was completed at a resolution of 4 cm^{-1} using an accumulation of 32 scans. The FTIR spectra were then collected using the Coherent Fourier Transform (CFT) method, while the inert purging gas was N_2. A KBr pellet was also introduced to each sample for analysis. These samples were fabricated as a disc-shaped translucent sample following the specifications outlined in ASTM E1252-98. The KBr pellet also underwent a degassing process to aggregate the sample particles efficiently. Consequently, the FTIR analysis allowed for the assessment of the chemical bonds and functional groups present in materials by examining the absorption of infrared light at specific frequencies.

2.2.4 SEM test

An SEM instrument (JSM IT-200) was used to analyse the morphology, chemical composition, crystalline structure, and orientation of the samples. This instrument could assess the position of the material on the designated surface (see Fig. 4). The instrument involved a concentrated high-energy electron beam, which caused the surfaces of the materials to generate numerous signals. Furthermore, the height offset was calibrated to handle tall samples before the sample loading process. Each of these samples necessitated a maximum diameter of 150 mm and a height of 48 mm. The procedure of evacuating the chamber was initiated after acquiring the optical image (holder graphics). This process entailed completing the designated observation area, condition settings, and image adjustments. The image magnification ranged from

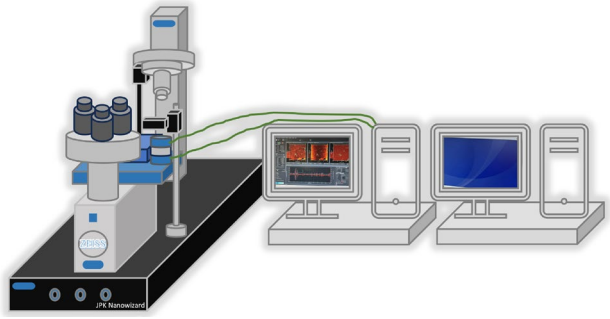

Fig. 6 The AFM test involving the JPK NanoWizard tool

× 5 to × 300,000, depending on the accelerating voltage (0.5 kV to 30 kV). Consequently, the SEM results were obtained for the individual waste materials and various hybrid asphalt binder mixtures (0%, 3%, 6%, and 9%). Figure 5 illustrates the positionings of the hybrid asphalt binder and mixture in the SEM instrument.

2.2.5 AFM test

The surface topography image was acquired through interaction measurement be-tween a sharp tip and the scanned surface of the cantilever. This technique was performed with the tapping mode in the JPK Nanowizard tool, which provided safe-guards against potential harm to the sample (see Fig. 6). A rectangular silicon tip was utilised in the tapping mode (topography and phase) at 27°C. This study employed a cantilever with a spring constant of 40 N/m, a thickness of 4 m, a length of 125 m, and a width of 30 m. Each sample scan involved a scan size of 20 µm × 20 µm and 40 µm × 40 µm.

2.3 Preparation of the hybrid asphalt binder mixtures

This study used a blending method to generate four hybrid asphalt binder samples (0%, 3%, 6%, and 9%). The technique involved a high-shear mixer to achieve a uniform asphalt blend at 1500 rpm and 160°C for 1 h. A mixture containing 25 µm POFA, garnet waste, and sawdust was combined with the original asphalt in different proportions to create hybrid asphalt binder mixtures. The proportions used were 0% (control), 3%, 6%, and 9%. Figure 7 portrays the hybrid asphalt binder blending procedure, which the SEM and AFM instruments later examined. Meanwhile, Fig. 8 demonstrates the JPK Nanowizard and JSM-IT200 instruments characterising the various hybrid asphalt binder mixtures. Each sample was fabricated on a glass slide measuring 1 cm in diameter.

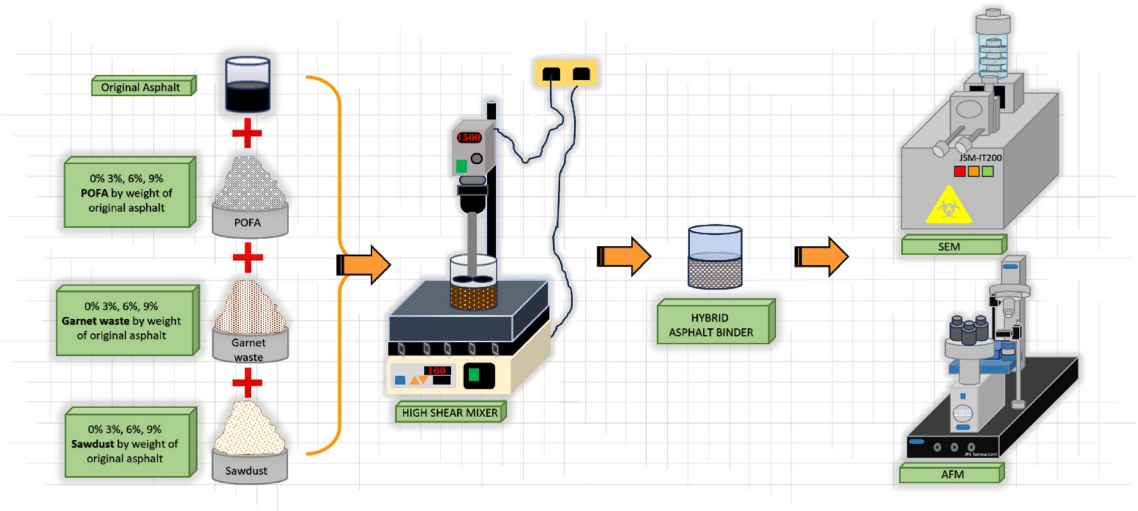

Fig. 7 The preparation of the hybrid asphalt binder and tested with SEM and AFM instruments

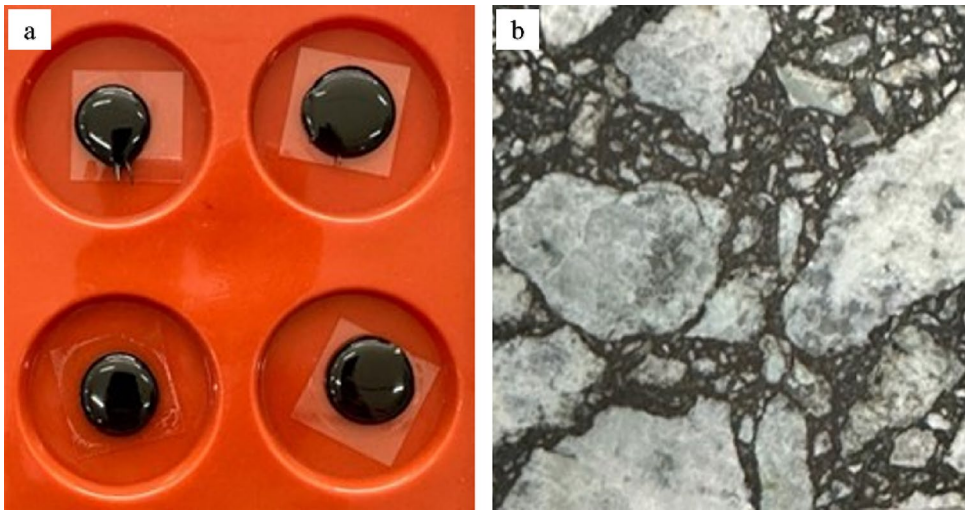

Fig. 8 The sample preparation processes of the **a** hybrid asphalt binder and the **b** hybrid asphalt mixture

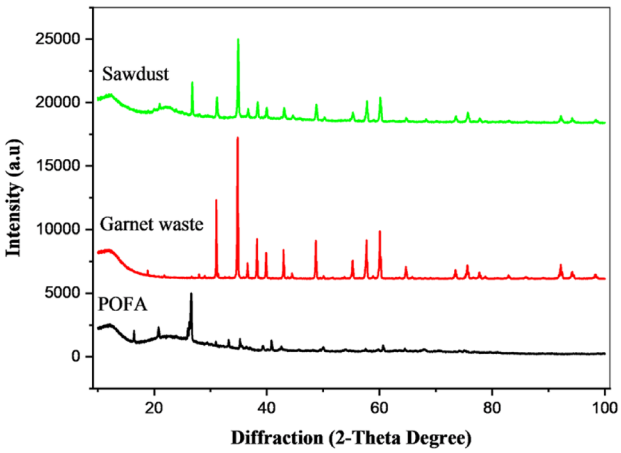

Fig. 9 The XRD diffraction patterns for POFA, garnet waste, and sawdust

3 Result and discussion

3.1 Chemical properties of waste materials

3.1.1 XRD

Figure 9 displays the XRD patterns of the POFA, garnet waste, and sawdust samples. The XRD pattern of POFA revealed that the highest peak intensity was located at 26.56°, indicating the presence of SiO_2. This observation suggested that SiO_2 was the primary constituent of the POFA [37, 38]. Alternatively, the average crystallite size (D) (represented as the peak width) of the highest intensity peak was 32.98 nm. The coefficient of determination value (R^2) for the POFA was also 0.87.

The XRD peaks of garnet waste displayed greater intensities compared to POFA and sawdust. Notably, the quartz in the garnet waste was highlighted by the peak at 34.82°. This significant peak verified the high SiO_2 and Fe_2O_3 levels in the XRF data (see Section 3.1.2). Thus, a high quartz content in the garnet waste was concluded, while an appreciable silica content was demonstrated in garnet waste and POFA. These findings indicated that POFA could perform comparably to garnet waste in asphalt mixtures. Another component detected during the peak analysis was observed at 92.1° corresponding to Fe and Al. The R^2 value for the intensity of garnet waste was 0.94. The D value is also 37.27 nm using the Scherrer formula as follows (see Eq. 1):

$$D = \frac{k\lambda}{\beta \cos \theta}, \tag{1}$$

Table 4 Chemical composition summary of the XRF results for POFA, garnet waste, and sawdust

Chemical compound	Waste materials (%)		
	POFA	Garnet waste	Sawdust
SiO_2	62.81	27.13	4.61
Fe_2O_3	4.77	44.97	3.08
CaO	2.99	1.89	69.65
Al_2O_3	23.92	17.73	0.00
K_2O	1.80	0.01	6.83
MgO	0.69	4.90	0.00
P_2O_5	0.79	0.41	2.96
SO_3	0.23	0.06	1.64

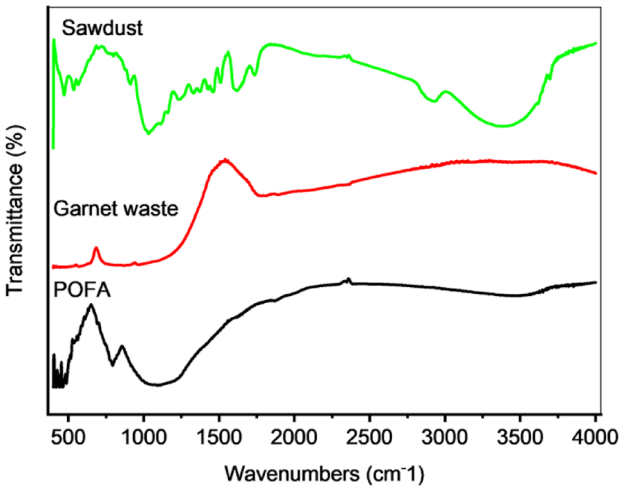

Fig. 10 The FTIR results for POFA, garnet waste, and sawdust

where D is the crystallite size (nm), k is the constant factor (0.62–2.08), λ is the wavelength (nm), β is the full width at half maximum of peaks (rad), and θ is the angle.

Considering that the disordered nature of the sawdust pattern was observed in the XRD pattern, several amorphous phases (lignin and hemicelluloses) were predicted [15]. The sole crystalline phase detected was cellulose, consisting of a distinct peak at 26.56°, a broad peak from 20° to 25°, and a wideband peak at 35°. A crystallite size of 29.81 nm was then recorded during the sawdust peak analysis. The peak intensity also presented an R^2 value of 0.88, demonstrating a strong correlation with the size, shape, orientation, and degree of order of the material. Consequently, the sawdust exhibited single and polycrystalline properties, indicating that it is a crystalline substance. Overall, the XRD data offered valuable information about the composition and crystalline structure of waste materials, aiding in comprehending their potential impact when employed in modified asphalt binders.

3.1.2 XRF

The XRF test yielded information regarding the chemical compositions of POFA, garnet waste, and sawdust. Table 4 reveals that the predominant oxide group in POFA is SiO_2, accounting for 62.81% of the composition. Subsequently, Al_2O_3 was the second most crucial oxide group at 23.92%. Additional oxide groups identified in POFA included Fe_2O_3 (4.77%), CaO (2.99%), K_2O (1.8%), and P_2O_5 (0.79%). Meanwhile, the predominant constituent in garnet waste was Fe_2O_3 (44.97%). Other reported oxide groups in garnet waste included SiO_2 (27.13%), Al_2O_3 (17.73%), MgO (4.90%), and CaO (1.89%). These findings aligned with garnet waste related studies, in which Fe_2O_3 was consistently recognised as the primary constituent [8, 39, 40].

The highest value for sawdust was CaO (69.65%). Conversely, K_2O and SiO_2 recorded content values of 6.83% and 4.61%, respectively. Sawdust typically possesses elevated SiO_2 and CaO levels, while the Fe_2O_3 content is minimal. Therefore, the XRF data offered insights into the elemental makeup of waste materials, which was crucial for comprehending their potential consequences and behaviour in different applications.

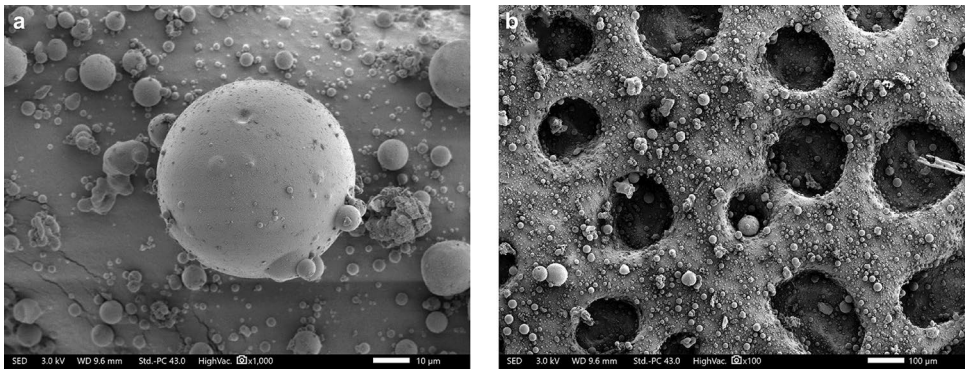

Fig. 11 The SEM images of POFA at **a** high and **b** low magnifications

Table 5 Percentage summary of the component masses in POFA, garnet waste and sawdust using EDX analysis

Element (%)	Fe	O	Si	Al	Mg	C
POFA	–	100	–	–	–	–
Garnet waste	37.82	33.73	12.61	8.42	4.89	2.53
Sawdust	–	47.04	–	–	–	52.96

3.1.3 FTIR

The FTIR analysis produced data on the specific functional groups present in the waste materials. Numerous absorption bands were documented for POFA at different wavenumbers (see Fig. 10). The prominent peaks were detected at 420 cm^{-1}, 443 cm^{-1}, 464 cm^{-1}, 487 cm^{-1}, 563 cm^{-1}, 794 cm^{-1}, 1016 cm^{-1}, 1089 cm^{-1}, 1125 cm^{-1}, and 3468 cm^{-1}. Specifically, a significant peak at 1089 cm^{-1} corresponded to the Si–O stretching of the Si–O–Si bonds. On the contrary, the peaks at 420 cm^{-1}, 443 cm^{-1}, 464 cm^{-1}, and 487 cm^{-1} were indicative of asymmetric bending vibrations of Si–O–Si. The peak at 794 cm^{-1} also suggested the occurrence of Si–O symmetric stretching and aromatic C–H bending vibrations. Likewise, the peak at 3468 cm^{-1} was related to the O–H stretching vibrations concerning water molecules absorbed in the binder. The peak at 1125 cm^{-1} also implied the aliphatic branches in the C–O–C stretching group. These findings aligned with the high SiO_2 content of POFA, which was demonstrated in the XRF study.

The FTIR spectra for the garnet waste recorded absorption bands at wavenumbers of 1782 cm^{-1}, 966 cm^{-1}, 873 cm^{-1}, 568 cm^{-1}, 510 cm^{-1}, 502 cm^{-1}, 487 cm^{-1}, 472 cm^{-1}, 455 cm^{-1}, 444 cm^{-1}, 436 cm^{-1}, 423 cm^{-1}, and 414 cm^{-1}. Notably, the significant peak at 1782 cm^{-1} indicated the C=O stretching in the oxygenic groups. The peaks at 966 cm^{-1} and 873 cm^{-1} in the fingerprint region also indicated the occurrence of active stretching and bending vibrations concerning the Si–O bond. In contrast, the peak at 1782 cm^{-1} corresponded to the stretching vibrations of Fe_2OH, demonstrating the unique garnet waste composition. Meanwhile, the 568 cm^{-1} to 455 cm^{-1} peaks were attributed to Si–O–Al and Si–O–Si bending vibrations, respectively.

The FTIR analysis of sawdust indicated the presence of several functional groups, which the absorption bands included O–H (3400 cm^{-1}), C–H (3000 cm^{-1}), C=O stretching (1730 cm^{-1}), and C–H bending (1000 cm^{-1}). The peak at 3385 cm^{-1} was attributed to cellulose and lignin phenol clusters. Likewise, the peak at 2930 cm^{-1} corresponded to the asymmetric vibrations of the CH_2 and $–CH_3$ groups. The peak at 1621 cm^{-1} also implied the presence of carboxylate clusters. Additional absorption bands corresponded to C=O stretching, C–C stretching, C–H bending, and C–O stretching. Nevertheless, the –H and aliphatic C–H functional groups were also observed. Overall, the FTIR data offered valuable information regarding the functional groups and molecular structures in waste materials. This outcome could aid in comprehending their chemical properties and probable interactions within asphalt mixtures.

3.2 Microstructural characterisations of waste materials

3.2.1 SEM

The SEM study revealed valuable information regarding the surface characteristics and structure of the waste materials. Figure 11 illustrates the particles in POFA as a bonded cloud of smoke, white in colour, with a rough and porous

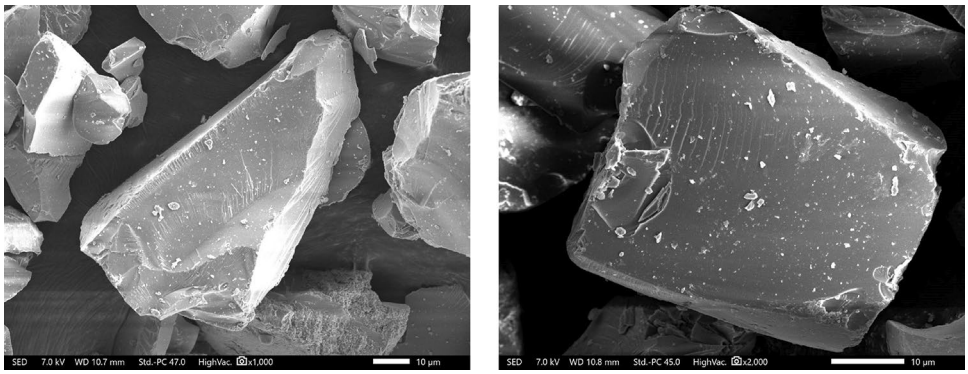

Fig. 12 The SEM images of garnet waste at different angles

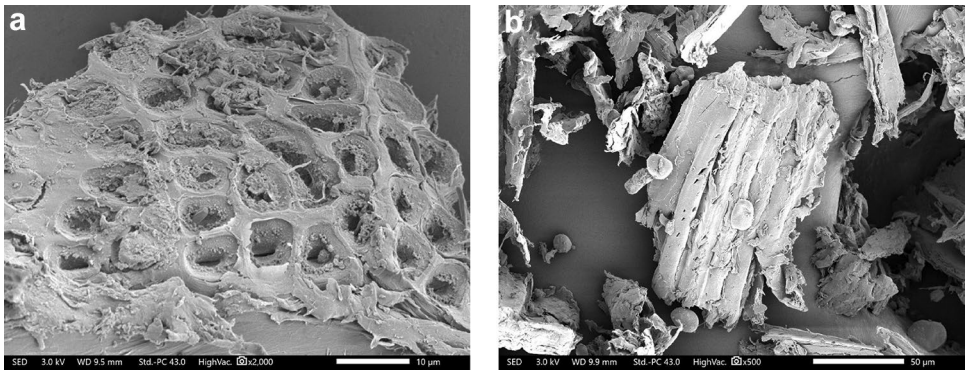

Fig. 13 The SEM images of sawdust at **a** high and **b** low magnifications

surface. The dimensions and morphology of the particles exhibited variations contingent upon the pro-cessing conditions employed. Darker spots also implied the voids in the microstructure. When Energy Dispersive X-ray (EDX) analysis was performed, the primary chemical element in POFA was O, constituting 100% of its weight (see Table 5). This observation corresponded to SiO_2 composition, which was also identified as the predominant component in XRF and XRD investigations. The SEM observations revealed that the surface characteristics appeared white and crystalline due to SiO_2. Thus, this discovery was supported by the XRF study, which confirmed a substantial amount of SiO_2 in POFA.

The SEM image of the garnet waste displayed crystalline particles characterised by irregular forms and a surface ranging from smooth to slightly rough (see Fig. 12). When the magnification was 500 kx, the particles appeared highly dense. Several chemical elements were detected in the EDX analysis, including C, O, Mg, Al, Si, and Fe (see Table 5). The element with the most significant weight percentage was Fe, which accounted for 37.82% of the total weight. This outcome was followed by O (33.73%), Si (11%), and Al (8%). The XRD examination results also confirmed the almandine ($Al_2Si_3O_{12}$) in the garnet waste, which was consistent with these findings. The high $Al_2Si_3O_{12}$ content enhanced mechanical properties and a more refined pore structure in the modified asphalt binder. Meanwhile, CaO and MgO suggested that the asphalt binder and mixture exhibited favourable performance and strong bonding capabilities.

The SEM image of sawdust highlighted unevenly shaped and amorphous particles exhibiting a rough and porous surface (see Fig. 13). Nonetheless, woodworking waste products could influence the size and shape of the particles. The EDX examination indicated that sawdust mainly consisted of O (47 %) and C (53 %) (see Table 5). Therefore, the EDX and XRF tests revealed a strong positive correlation, suggesting a significant amount of CaO (≥ 70%) in the sawdust. Overall, the SEM results presented substantial insights into the surface characteristics and chemical compositions of waste materials. This knowledge enhanced the understanding of their potential attributes and how they may behave when integrated into asphalt mixtures.

3.2.2 AFM

Figures 14, 15 and 16 depict the AFM topography images of the three waste components in the individual waste-modified asphalt binder samples: 3% POFA, 3% garnet waste and 3% sawdust. These samples revealed three distinctive phases, significantly affecting the AFM images. Consequently, the catana phase amount increased by 20%, 40%,

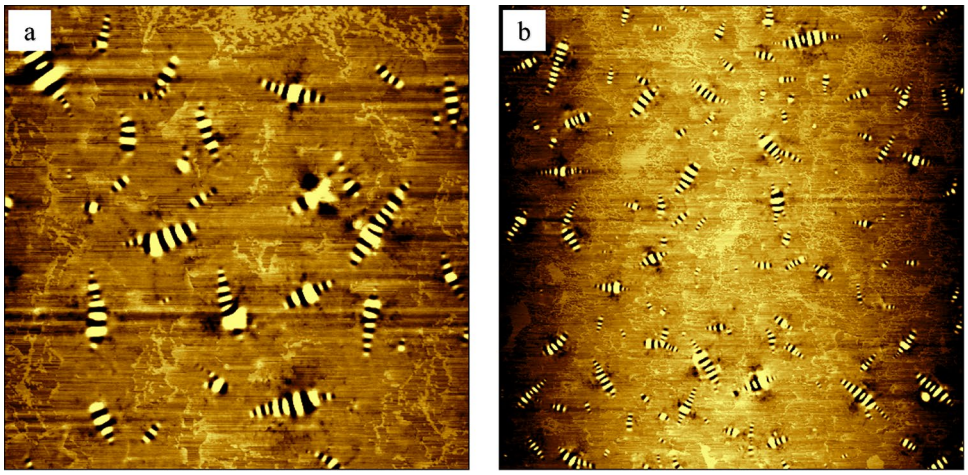

Fig. 14 The topography images of POFA using **a** 20 × 20 µm and **b** 40 × 40 µm scanning areas

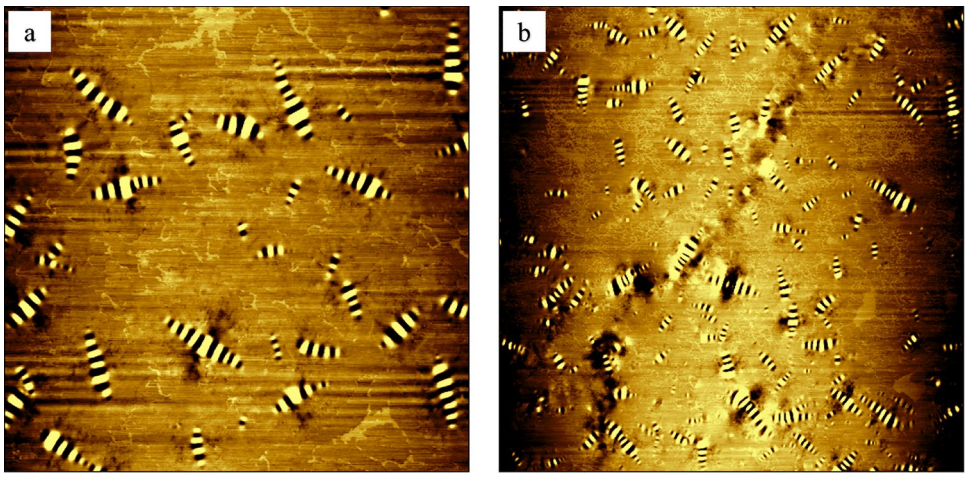

Fig. 15 The topography images of garnet waste using **a** 20 × 20 µm and **b** 40 × 40 µm scanning areas

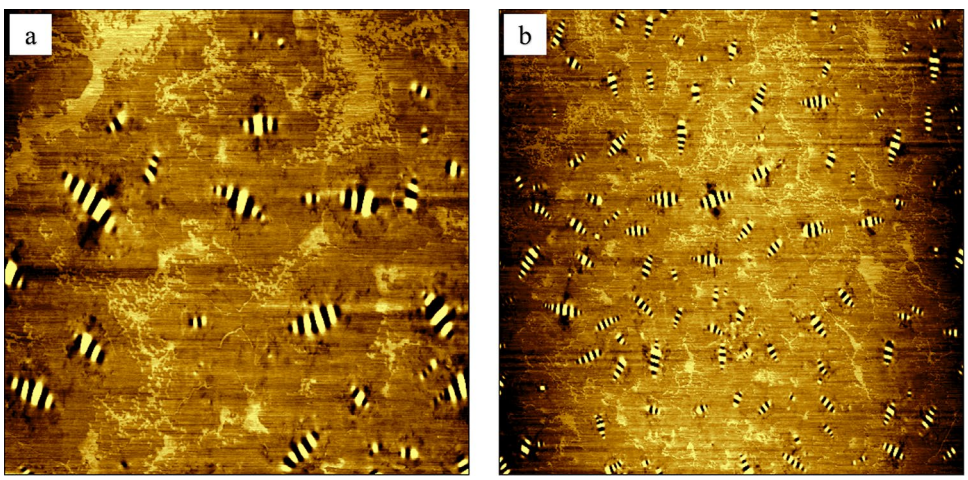

Fig. 16 The topography images of sawdust using **a** 20 × 20 µm and **b** 40 × 40 µm scanning areas

and 50% for the 3% POFA, 3% garnet waste and 3% sawdust, respectively. The catana phase exhibited a consistent size across all samples, measuring 7 µm to 12 µm in length and 1.0 µm to 1.5 µm in width. Similarly, the phase contrast between peri and para phases was inverted at more significant SiO_2 percentages (3% sawdust), resulting in a higher para phase. A study by Masri et al. [41] denoted that para phases were grouped as low stiffness while peri and catana

phases were categorised as high stiffness. Compared with the study by Ji et al. [42] adding 3% POFA and 3% garnet waste did not substantially impact the improvement of the asphalt binder.

3.3 Microstructural characterisations of hybrid asphalt binder and mixtures

3.3.1 SEM

Figures 17, 18, 19 and 20 showcase the morphological images of various hybrid asphalt binder mixtures (control, 3%, 6% and 9%). The surface of the aggregates exhibited noticeable voids and gaps. Improper bonding between the particles (irregular surface textures) was also presented due to the inadequate coating application and the prominent unevenness of the surface. Given that no discernible gaps between the aggregates were recorded after the modification process, the voids generated smaller sizes and produced a compact surface. Consequently, the 6% hybrid asphalt binder mixture demonstrated improved material bonding of the POFA, garnet waste, and sawdust components compared to the control sample. A significant surface exposure was also presented due to the extensive surface area of this mixture. The particles in the 6% hybrid asphalt binder mixture were uniformly distributed, establishing a cohesive bond among

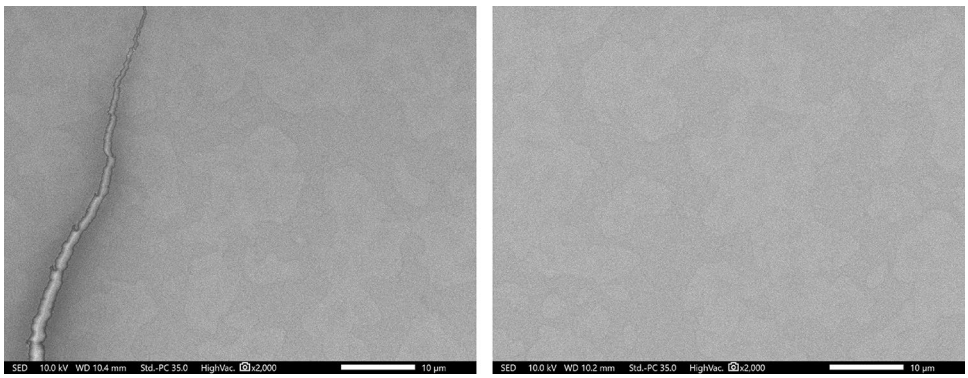

Fig. 17 The SEM images of the control asphalt at different angles

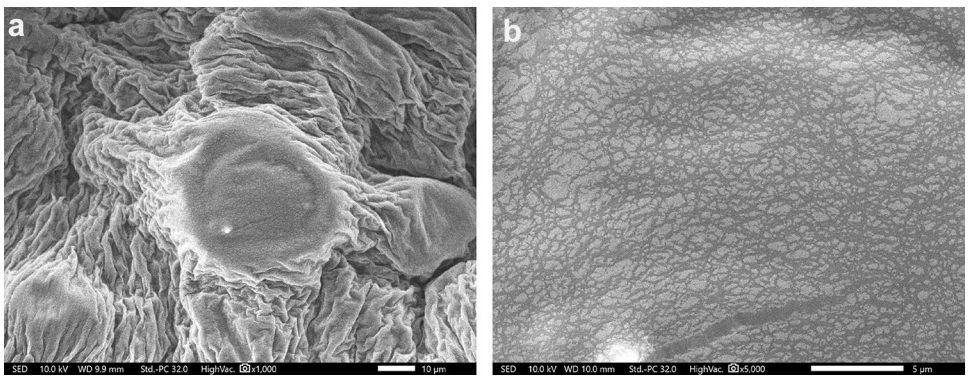

Fig. 18 The SEM images of the 3% hybrid asphalt binder mixture at **a** high and **b** low magnifications

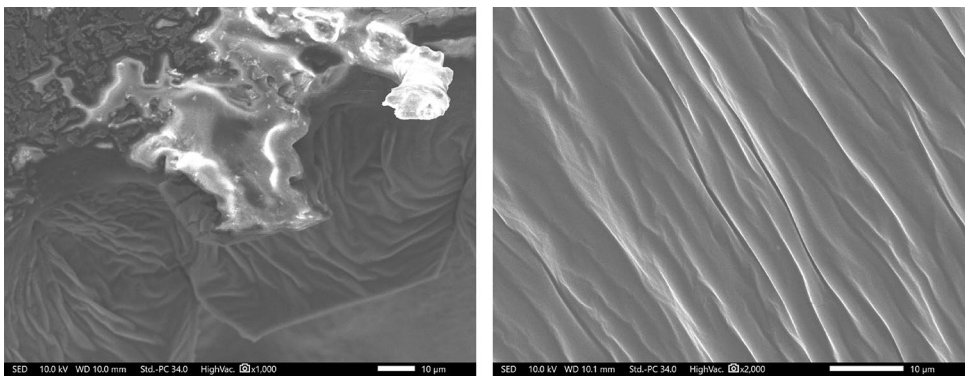

Fig. 19 The SEM images of the 6% hybrid asphalt binder at different angles

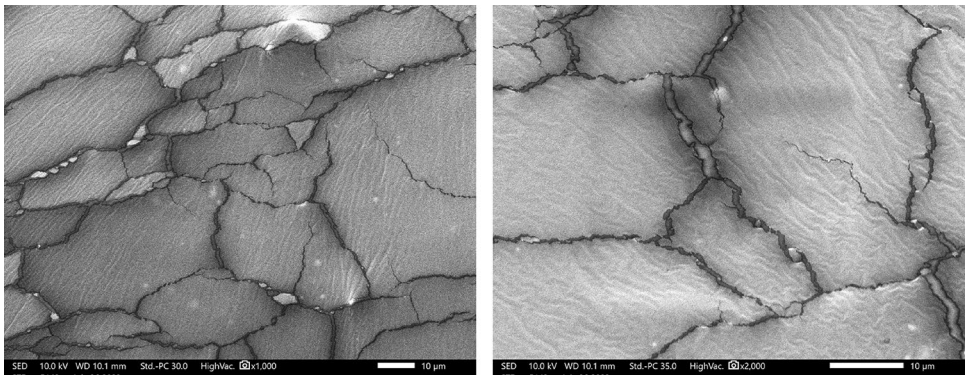

Fig. 20 The SEM images of the 9% hybrid asphalt binder at different angles

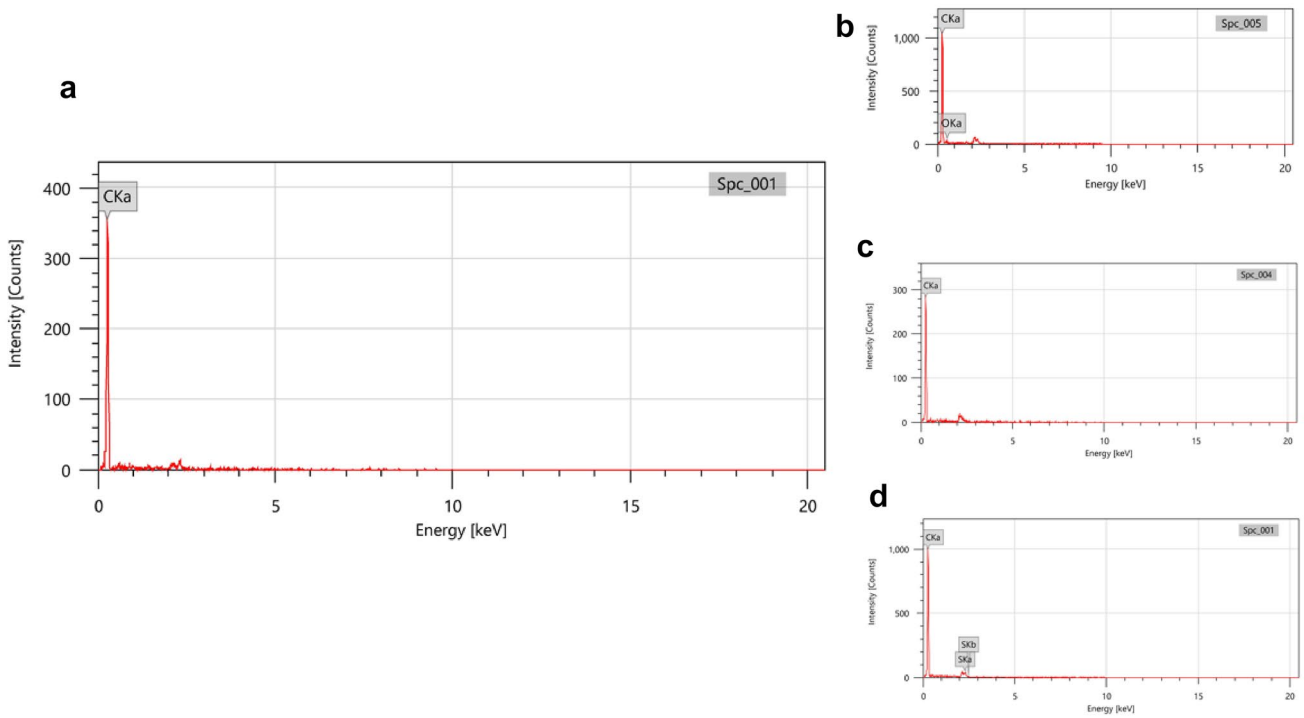

Fig. 21 The EDX patterns of the **a** control, **b** 3%, **c** 6%, and **d** 9% hybrid asphalt binders

the constituents. Meanwhile, the AFM investigation demonstrated that the particle interactions increased interfacial forces and decreased surface roughness. This finding improved the bonding characteristics of the 6% hybrid asphalt binder mixture. Therefore, the enhanced bonding of the 6% hybrid asphalt binder mixture produced a gap-filling and homogeneous coating, which presented greater strength.

The asphalt component identified the C peaks in the EDX graphs of the control, 3%, 6%, and 9% hybrid asphalt binders (see Fig. 21). Each hybrid asphalt mixture contained Si, Ca, and Al peaks, revealing the waste materials (POFA, garnet waste, sawdust) and the aggregates (see Fig. 22 and Table 6). Notably, the 3% and 6% hybrid asphalt binder mixtures included C, O, and Si as the primary contributors (C > O > Si). The 6% hybrid asphalt mixture produced a higher C (10% increment) and lower Si (29% reduction) with O (33% reduction) than the control. Nevertheless, the 9% hybrid asphalt binder mixture contributed the most inferior C content (C < Si < O). Although the control demonstrated lower C (15% reduction), it exhibited the highest Si and O levels among all samples.

The hybrid asphalt binder mixtures displayed a uniform surface due to the high C content, which promoted strong bonding between the hybrid materials and aggregates. Alternatively, the lower Si content was ascribed to reduced exposure of the aggregate surfaces resulting from the efficient coverage of aggregate particles in the hybrid asphalt binder mixtures. All the hybrid asphalt binder mixtures also demonstrated smaller voids and gaps between the

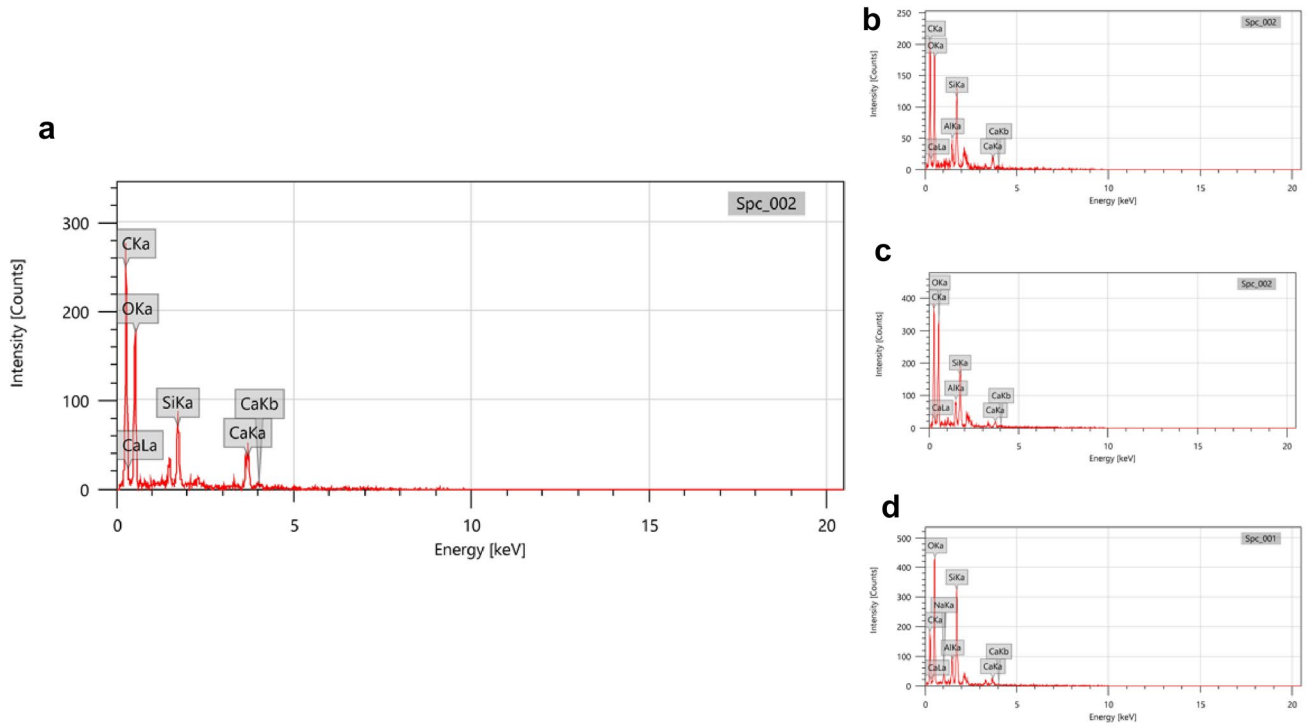

Fig. 22 The EDX patterns of the **a** control, **b** 3%, **c** 6%, and **d** 9% hybrid asphalt mixtures

Table 6 Mass percentage summary of the hybrid asphalt mixtures from the EDX analysis

Element (%)	C	O	Si	Ca	Al
0	37.09	34.27	8.42	20.21	–
3	44.86	34.40	12.44	3.69	4.61
6	39.47	32.97	14.45	9.04	4.07
9	25.74	39.96	18.98	8.36	4.02

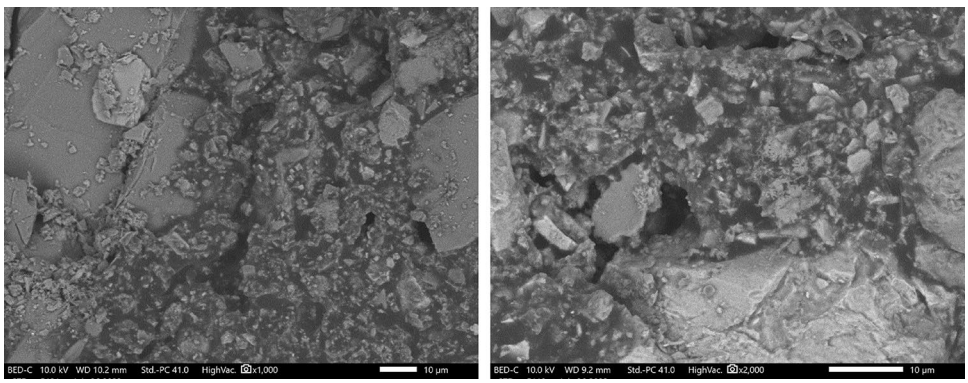

Fig. 23 The SEM images of the control asphalt at different angles

aggregates. This outcome produced lower oxidation and an accelerated ageing process of the mixture [43]. Overall, the hybrid materials (POFA, garnet waste, and sawdust) in the asphalt mixture could enhance the sustainability and performance of asphalt materials. Simultaneously, this process could reduce the negative environmental impact associated with traditional materials. The results from analysing the SEM-EDX instrument provided valuable insights into the elemental composition and distribution of the hybrid asphalt mixtures. Therefore, the 6% hybrid asphalt binder mixture demonstrated its capacity to serve as a replacement component.

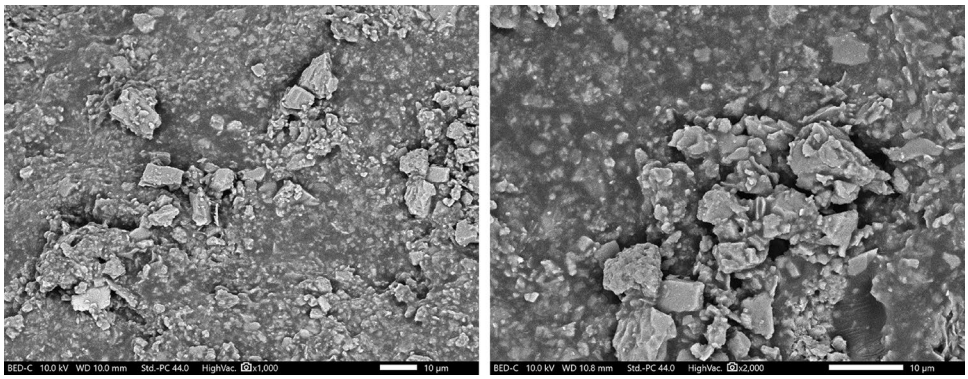

Fig. 24 The SEM images of the 3% hybrid asphalt mixture at different angles

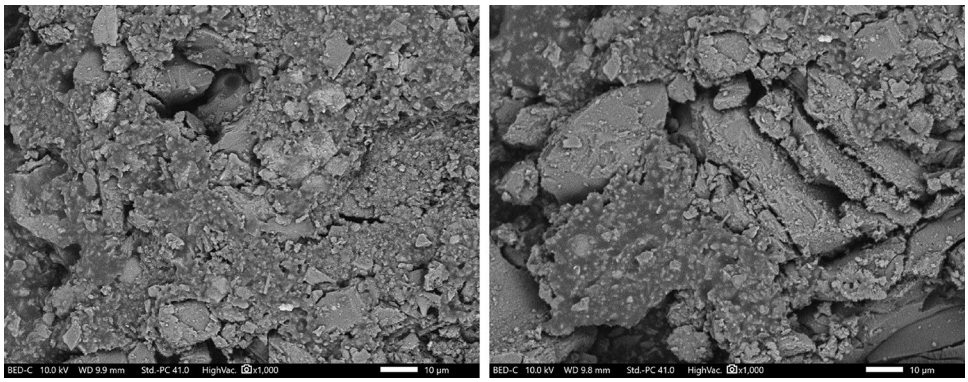

Fig. 25 The SEM images of the 6% hybrid asphalt mixture at different angles

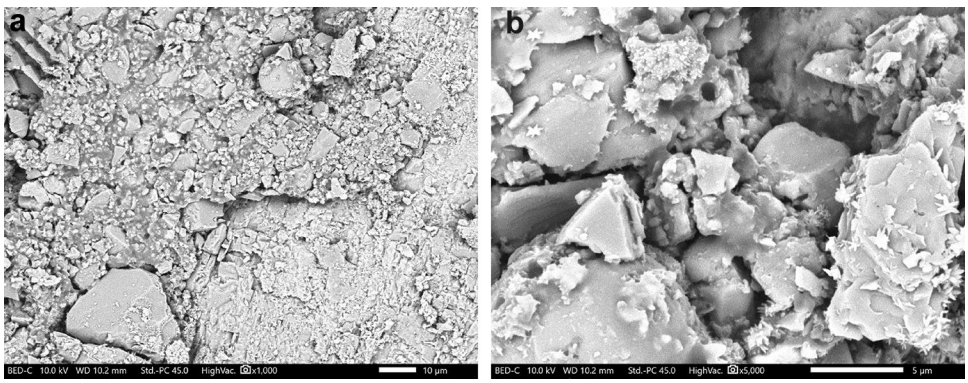

Fig. 26 The SEM images of the 9% hybrid asphalt mixture at **a** low and **b** high magnifications

Figures 23, 24, 25 and 26 portray the morphological images of the control, 3%, 6%, and 9% hybrid asphalt mixtures. These images revealed obvious gaps and cavities on the aggregate surface. An insufficient coating approach also produced uneven surface textures and a noticeable roughness, causing unsatisfactory particle bonding. Following the modification, no discernible gaps between the aggregates were observed. Thus, the voids decreased in size and formed a dense surface (see Fig. 25). These outcomes indicated that the 6% hybrid asphalt mixture exhibited improved material bonding of the POFA, garnet waste, and sawdust components compared to the control. The wide surface area of the 6% hybrid asphalt mixture also documented substantial surface exposure. Furthermore, the 6% hybrid asphalt mixture particles were uniformly distributed, establishing a solid connection between the components. Meanwhile, the AFM investigation revealed that the bonding properties of the 6% hybrid asphalt mixture were enhanced due to the higher interfacial forces and reduced surface roughness resulting from particle interactions. Consequently, the improved bonding of the hybrid asphalt mixture resulted in a uniform and gap-free surface, thereby enhancing its strength.

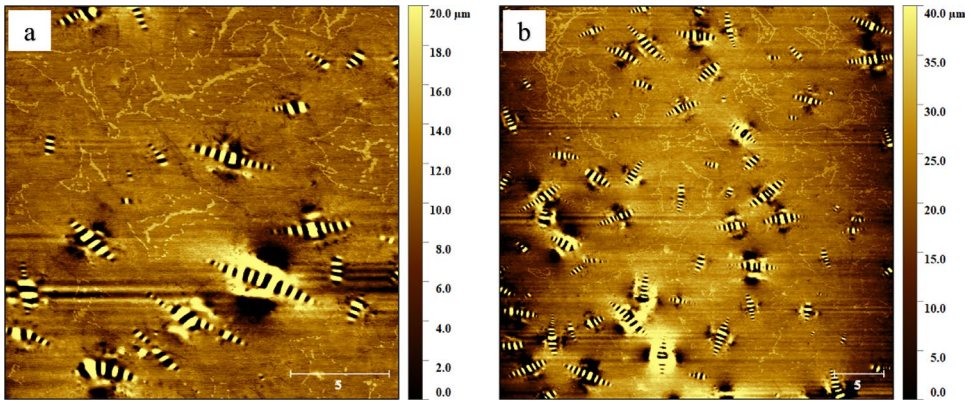

Fig. 27 The AFM images for **a** 20 × 20 µm **b** 40 × 40 µm scanning areas of the control asphalt

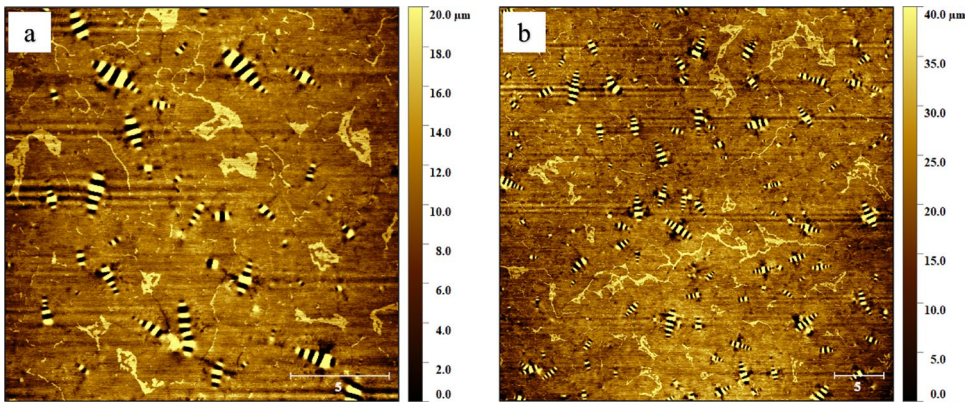

Fig. 28 The AFM images for **a** 20 × 20 µm **b** 40 × 40 µm scanning areas of the 3% hybrid asphalt binders

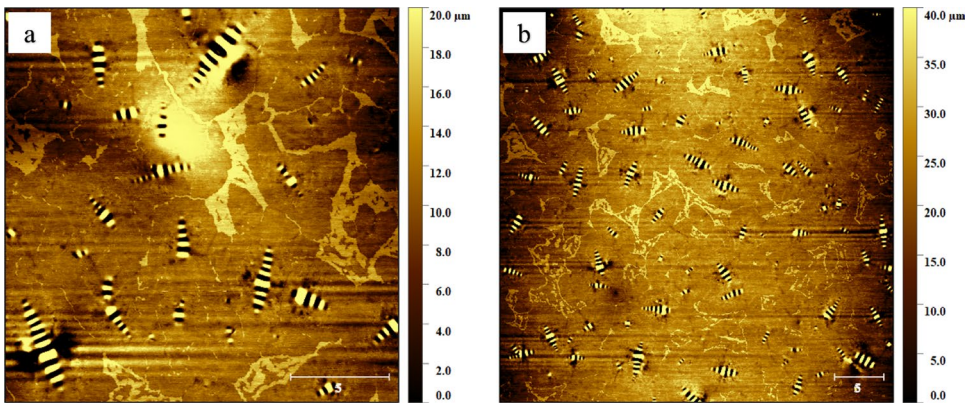

Fig. 29 The AFM images for **a** 20 × 20 µm **b** 40 × 40 µm scanning areas of the 6% hybrid asphalt binders

3.3.2 AFM

An AFM instrument was used to analyse the topographical features of the hybrid asphalt binders. This study evaluated the surface roughness of the control, 3%, 6%, and 9% hybrid asphalt binders by scanning two different areas (20 µm × 20 µm and 40 µm × 40 µm). Consequently, the hybrid asphalt binder topographies consisted of three unique phases: the bee structure (catana phase), the scattered domain (dark region or peri phase), and the flat matrix (light region or para phase) [41, 44]. Figures 27, 28, 29 and 30 depict the phase images of the control, 3%, 6%, and 9% hybrid asphalt binders. These images showcased a clear structural arrangement resembling a bee structure or catana phase dispersed within the matrix. Compared to the control, the bee structures of the 3%, 6%, and 9% hybrid asphalt binders were redesigned and downsized. The 6% hybrid asphalt binder also acquired a higher dispersed phase. This observation was attributed to a chemical interaction between the constituent materials and the asphalt component, resulting in the elastomeric

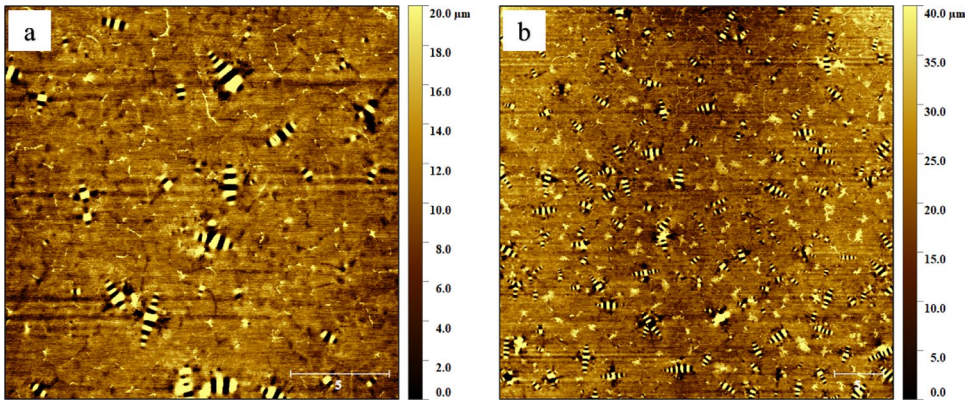

Fig. 30 The AFM images for **a** 20 × 20 µm **b** 40 × 40 µm scanning areas of the 9% hybrid asphalt binders

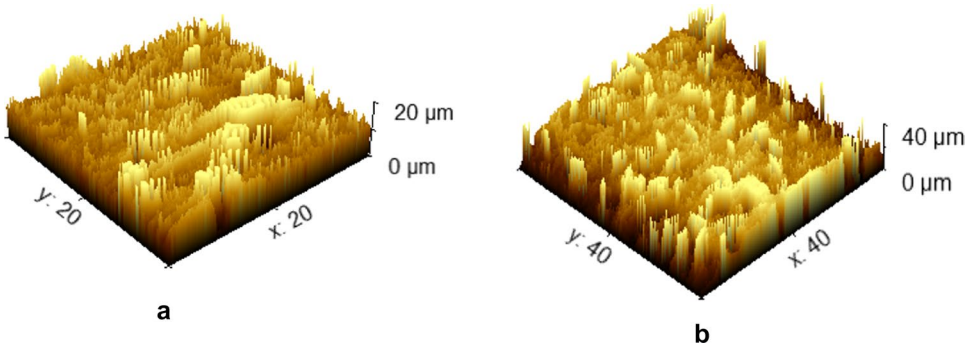

Fig. 31 The 3D views of the **a** 20 × 20 µm **b** 40 × 40 µm scanning areas of the control asphalt

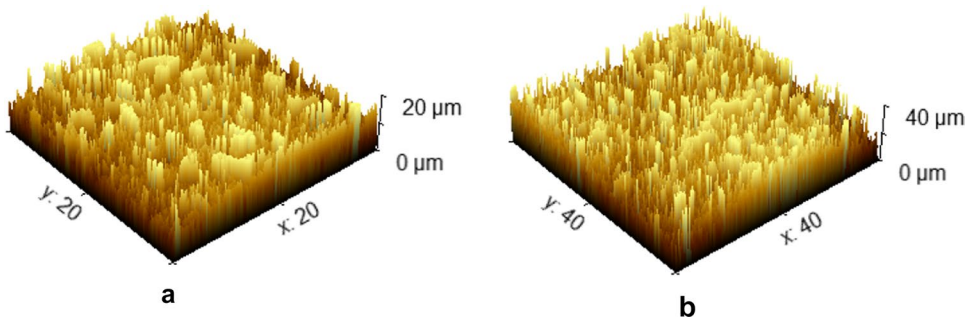

Fig. 32 The 3D views of the **a** 20 × 20 µm **b** 40 × 40 µm scanning areas of the 3% hybrid asphalt binders

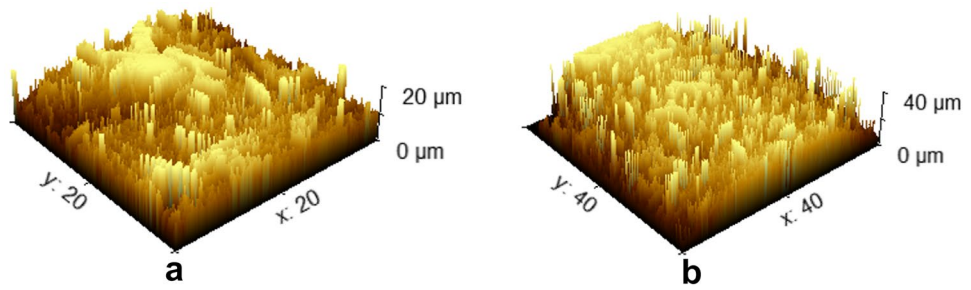

Fig. 33 The 3D views of the **a** 20 × 20 µm **b** 40 × 40 µm scanning areas of the 6% hybrid asphalt binders

material swelling and altering the elastic characteristics of the entire bituminous matrix [45, 46]. The distributions of dark region zones in the 3%, 6%, and 9% hybrid asphalt binder mixtures were also inconsistent. Conversely, the control asphalt demonstrated constant dispersion, proving the consistent distribution of hybrid asphalt in the asphalt binders.

The hybrid materials (POFA, garnet waste, and sawdust) influenced the consistent dispersion region. Within this region, the 6% hybrid asphalt binder demonstrated the smallest bee structure and showcased a uniform distribution

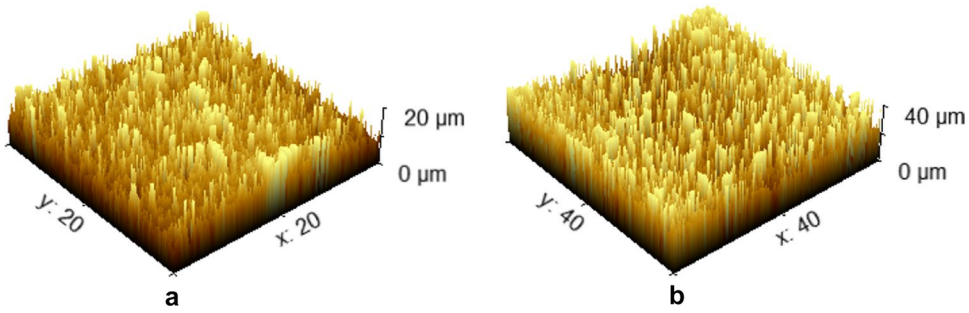

Fig. 34 The 3D views of the **a** 20 × 20 µm **b** 40 × 40 µm scanning areas of the 9% hybrid asphalt binders

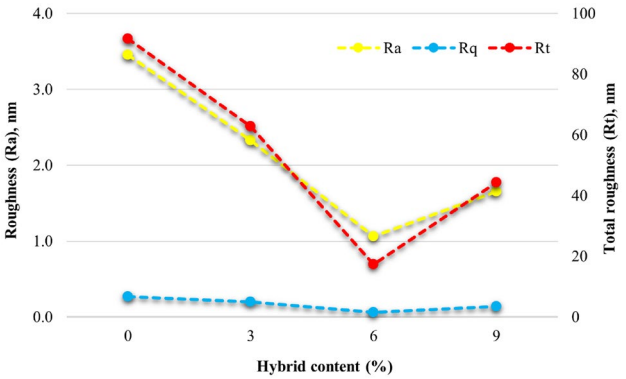

Fig. 35 The surface roughness values of the control, 3%, 6%, and 9% hybrid asphalt binders

of domains. Typically, the presence of asphaltenes helps to form bee structures. Thus, the hybrid asphalt binders (3%, 6%, and 9%) with reduced aromatics content created small and homogenous bee structures. These structures were also influenced by the surface roughness of the asphalt [47]. Figures 31, 32, 33 and 34 illustrate the 3D view scanning areas (20 µm × 20 µm and 40 µm × 40 µm) of the control, 3%, 6%, and 9% hybrid asphalt binders. Meanwhile, the study demonstrated that the particle interactions promoted increased interfacial forces and decreased surface roughness. This process improved the bonding capabilities of the 6% hybrid asphalt binder (see Fig. 33). Consequently, the enhanced bonding of the hybrid asphalt binders led to filling gaps and forming a uniform covering, which improved strength.

Figure 35 displays the average roughness (Ra), root mean square roughness (Rq), and total roughness (Rt) for the control, 3%, 6%, and 9% hybrid asphalt binder. The Ra parameter is frequently utilised in surface roughness analysis to provide a number that does not consider specific peaks and valleys. In contrast, the Rq parameter is highly sensitive to variations in peak and valley values. Likewise, the overall vertical difference between the highest and lowest points is denoted as Rt. All these values (Ra, Rq, Rt) of the 3%, 6%, and 9% hybrid asphalt binder were comparatively lower than the control asphalt. An initial decline was detected until the 6% hybrid asphalt binder, followed by a further increase until the 9% hybrid asphalt binder. This trend implied that the 6% hybrid asphalt binder exhibited a lower surface roughness value than the other samples. The lower bee structure size and the uniformity of the peri phase region in the 6% hybrid asphalt binder contributed to the enhanced smoothness of the hybrid asphalt surface.

Effective bonding between the hybrid materials and the asphalt matrix was observed due to the uniform distribution of the hybrid materials (POFA, garnet waste, and sawdust) within the hybrid asphalt matrix. This uniform dispersion of the hybrid components led to improved bonding between the hybrid asphalt binders and aggregates. The surface roughness analysis in the stability test displayed the highest strength, suggesting enhanced bonding between the hybrid asphalt binder and the aggregate. Figure 36 illustrates the 3D views of the control, 3%, 6%, and 9% hybrid asphalt binder. The peaks and valleys on the surfaces of the hybrid asphalt binder indicated the formation of bee structures. Specifically, the 6% hybrid asphalt binder resulted in a lower amount and smaller height of the bee structure than the control asphalt. Thus, the bonding capabilities of the 6% hybrid asphalt binder were significantly enhanced by its roughness. This procedure enhanced the bonding between the asphalt and the aggregates.

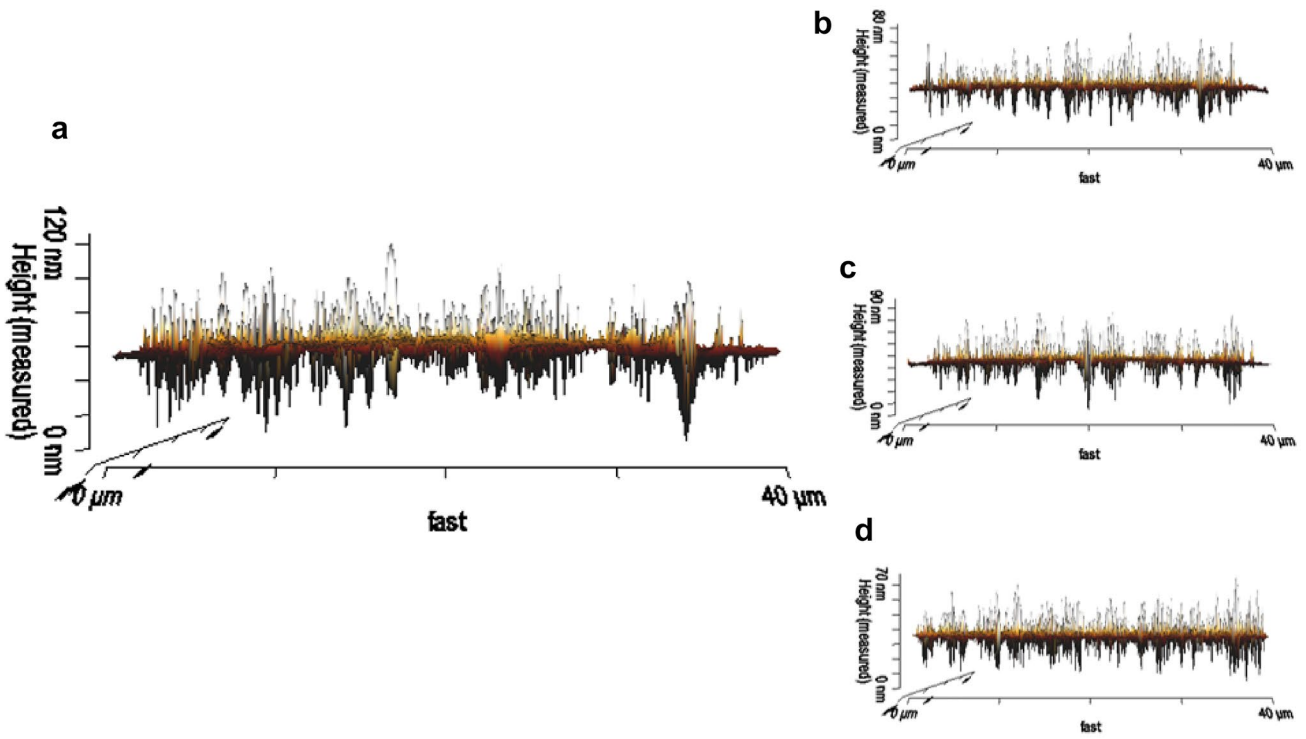

Fig. 36 The 3D views of the **a** control, **b** 3%, **c** 6%, and **d** 9% hybrid asphalt binders with 40 × 40 µm dimension sizes

4 Conclusions

This study successfully investigated the chemical characteristics and microstructure analysis of individual wastes and various hybrid asphalt binder and mixtures. The XRD and XRF analyses demonstrated that the chemical compositions of POFA, garnet waste, and sawdust contained high amounts of SiO_2, Fe_2O_3, and CaO, respectively. The morphologies of POFA exhibited a clustered arrangement resembling smoke clouds, while garnet waste and sawdust produced irregularly shaped particles with a porous surface (primarily composed of oxygen as indicated by the EDX analysis). This result suggested that all three waste types presented improved fatigue resistance due to irregular shapes and sizes. The FTIR analysis also confirmed the presence of significant SiO_2 concentration in POFA, garnet waste, and sawdust, which consistently supported previous studies. The SEM analysis demonstrated that the 6% hybrid asphalt binder and mixture exhibited a dense and homogeneous structure, indicating a strong bonding between the constituent materials. Therefore, this mixture was better than the control sample. The AFM investigation revealed that the 6% hybrid asphalt binder and mixture acquired the lowest surface roughness, indicating a strong bonding between the asphalt and aggregates. The asphaltene amount increased, leading to a more pronounced differentiation between phases as the percentage of hybrid content grew. Thus, modifying hybrid asphalt led to a notable impact and reduced the observed number of bee structures. The topographical and surface characteristics of the wastes and hybrid asphalt binder and mixtures were successfully performed using AFM and SEM. The AFM study demonstrated that incorporating hybrid materials as an additive facilitated a novel structure on the original hybrid asphalt binder surfaces. Observations also revealed that the combination impacted the binder, causing changes in the size of the bee structure. Furthermore, the hybrid asphalt concentration influenced the chemical and morphological behaviour of the hybrid asphalt binder mixtures. The 6% hybrid asphalt binder and mixture highlighted a significant improvement in the performance of the hybrid asphalt binder and mixtures. This improvement was attributed to the optimised density, enhanced stability, improved bonding, and interfacial solid bonding. Overall, the POFA, garnet waste, and sawdust components in road construction successfully exhibited promising enhancements in pavement performance, aligning with the overarching objectives of waste reduction and environmental sustainability in the infrastructure industry.

Author contributions W.N.H.M.S: Conceptualisation, methodology, formal analysis, investigation, writing—original draft preparation, writing—review and editing, R.P.J: Conceptualisation, validation, data curation, supervision, funding acquisition, K.A.M: Resources, project administration, K.S: validation, data curation, A.D: Resources, Conceptualisation.

Funding This research was funded by the Universiti Malaysia Pahang Al-Sultan Abdullah Post Graduate Research Grant (PGRS) (grant number: PGRS2303117).

Data availability The data used to support the findings of this study are available from the corresponding author upon request.

Declarations

Conflict of interest The authors declare that there is no conflict of interest regarding the publication of this article.

References

1. Yaro ANS, Sutanto MH, Habib NZ, Napiah M, Usman A, Jagaba AH, et al. Application and circular economy prospects of palm oil waste for eco-friendly asphalt pavement industry: a review. J Road Eng. 2022;2(4):309–31.
2. Hamada HM, Yahaya F, Muthusamy K, Humada A. Comparison study between POFA and POCP in terms of chemical composition and physical properties-Review paper. In: IOP Conference Series: earth and environmental science. institute of physics publishing; 2019.
3. Hamada HM, Thomas BS, Yahaya FM, Muthusamy K, Yang J, Abdalla JA, et al. Sustainable use of palm oil fuel ash as a supplementary cementitious material: A comprehensive review. Journal of Building Engineering. 2021;40.
4. Sani WNHM, Jaya RP, Masri KA. Performance of hybrid asphalt mixture through the stability and tensile strength. Open Civ Eng J. 2023. https://doi.org/10.21203/rs.3.rs-3932333/v1.
5. Akbas M, Ozaslan B, Iyisan R. Utilization of recycled concrete aggregates for developing high-performance and durable flexible pavements. Constr Build Mater. 2023;407:133479.
6. Cota J, Martínez-Lazcano C, Montoya-Alcaraz M, García L, Mungaray-Moctezuma A, Sánchez-Atondo A. Improvement in durability and service of asphalt pavements through regionalization methods: a case study in Baja California, Mexico. Sustainability (Switzerland). 2022;14(9):5123.
7. Hussein AA, Jaya RP, Abdul Hassan N, Yaacob H, Huseien GF, Ibrahim MHW. Performance of nanoceramic powder on the chemical and physical properties of bitumen. Constr Build Mater. 2017;156:496–505.
8. Hussein AA, Putra Jaya R, Yaacob H, Abdul Hassan N, Oleiwi Aletba SR, Huseien GF, et al. Physical, chemical and morphology characterisation of nano ceramic powder as bitumen modification. Int J Pavement Eng. 2021;22(7):858–71.
9. Joohari IB, Giustozzi F. Chemical and high-temperature rheological properties of recycled plastics-polymer modified hybrid bitumen. J Clean Prod. 2020;276:123064.
10. Stern S, Flyvbjerg B. Public and Social Sector Practice The emerging revolution in the road construction industry. 2021.
11. Mohd Hasan MR, Chew JW, Jamshidi A, Yang X, Hamzah MO. Review of sustainability, pretreatment, and engineering considerations of asphalt modifiers from the industrial solid wastes. J Traffic Transp Eng English Edition Chang'an Univ. 2019;6(3):209–44.
12. Modupe AE, Fadugba OG, Busari AA, Adeboje AO, Aladegboye OJ, Alejolowo OO, et al. Sustainability Assessment of the engineering properties of asphalt concrete incorporating pulverized snail shell ash as partial replacement for filler. In: IOP Conference Series: Earth and Environmental Science. 2021.
13. Abdulrahman S, Hainin MR, Satar MKIM, Hassan NA, Usman A. Rutting and moisture damage evaluation of warm mix asphalt incorporating POFA modified bitumen. Int J Eng Adv Technol. 2019;9(1):90–8.
14. Aletba SR, Hassan NA, Aminudin E, Putra Jaya R, Hussein AA. Marshall properties of asphalt mixture containing garnet waste. J Adv Res Mater Sci. 2018;43:22–7.
15. Fayissa B, Gudina O, Yigezu B. Application of sawdust ash as filler material in asphaltic concrete production. Civ Environ Eng. 2020;16(2):351–9.
16. Raja Zulkefli RNA, Yaacob H, Putra Jaya R, Warid MNM, Hassan N, Hainin MR, et al. Effect of different sizes of palm oil fuel ash (POFA) towards physical properties of modified bitumen. In: IOP Conference Series: Earth and Environmental Science. Institute of Physics Publishing; 2018.
17. Salami BA, Megat Johari MA, Ahmad ZA, Maslehuddin M, Adewumi AA. Impact of $Al(OH)_3$ addition to POFA on the compressive strength of POFA alkali-activated mortar. Constr Build Mater. 2018;190:65–82.
18. Alnahhal AM, Alengaram UJ, Yusoff S, Singh R, Radwan MKH, Deboucha W. Synthesis of sustainable lightweight foamed concrete using palm oil fuel ash as a cement replacement material. J Build Eng. 2021;35:102047.
19. Nandiyanto ABD, Oktiani R, Ragadhita R. How to read and interpret ftir spectroscope of organic material. Indonesian J Sci Technol. 2019;4(1):97–118.

20. Mulizar, Fazliah, Iskandar, Aiyub, Fauzi A. Effect of POFA as a replacement material on fly ash based geopolymer mortar. In: IOP Conference Series: Materials Science and Engineering. Institute of Physics Publishing; 2020.
21. Muttashar HL. Performance of self-compacting geopolymer concrete using spent garnet as sand replacement. In: Sustainable Construction Materials. 2019.
22. Usman KR, Hainin MR, Satar MKIM, Warid MNM, Usman A, Al-Saffar ZH, et al. A comparative assessment of the physical and microstructural properties of waste garnet generated from automated and manual blasting process. Case Stud Constr Mater. 2021;14:e00474.
23. Muttashar HL, Bin AN, Mohd Ariffin MA, Hussin MW. Microstructures and physical properties of waste garnets as a promising construction materials. Case Stud Constr Mater. 2018;8:87–96.
24. Karati S, Kumar RT. Assessment of temperature impact on SDA modified bituminous concrete by non-destructive test. Mater Today Proc. 2022;65:3417–23.
25. Ing S, Liew N, Cui Ng M, Jaya RP, et al. Influence of sawdust ash as filler in asphalt mixture. AIP Conference Proceedings AIP Publishing. 2023;2688(1).
26. Osuya DO, Mohammed H. Evaluation of sawdust ash as a partial replacement for mineral filler in asphaltic concrete. IFE J Sci. 2017;19(2):431.
27. Wang T, Rong H, Chen S, Zhou Y, Li J, Xiao Y, et al. TG- MS study on in-situ sulfur retention during the co-combustion of reclaimed asphalt binder and wood sawdust. J Hazard Mater. 2021;403:123911.
28. Couto GM, de Abreu L, Dessimoni A, Bianchi ML, Perígolo DM, Trugilho PF. Use of sawdust eucalyptus sp. in the preparation of activated carbons. Ciência e Agrotecnologia. 2012;36:69–77.
29. Ayuba S, Uche OA, Haruna S, Mohammed A. Durability properties of cement – saw dust ash (SDA) blended self compacting concrete (SCC). Niger J Technol. 2022;41(2):212–21.
30. Abdul Awal ASM, Abubakar I. Properties of concrete containing high volume palm oil fuel ash: a short -term investigation. Malaysian J Civ Eng. 2011;23(2):54–66.
31. Usman KR, Hainin MR, Mohd Satar MKI, Mohd Warid MN, Kamarudin SNN, Abdulrahman S. Palm oil fuel ash application in cold mix dense-graded bituminous mixture. Constr Build Mater. 2021;287:123033.
32. Salih MA, Farzadnia N, Demirboga R, Ali AAA. Effect of elevated temperatures on mechanical and microstructural properties of alkali-activated mortar made up of POFA and GGBS. Constr Build Mater. 2022;328:127041.
33. Ibrahim SAB, Korkmaz S, Cetin MH, Kartal F. Performance evaluation of the submerged abrasive water jet turning process for improving machinability of castamide. Eng Sci Technol, Int J. 2020;23(4):801–11.
34. Yuan Y, Zhu X, Chen L. Relationship among cohesion, adhesion, and bond strength: From multi-scale investigation of asphalt-based composites subjected to laboratory-simulated aging. Mater Des. 2020;185:108272.
35. García A, Moya JPA, Delgado JS, Sevilla AB, Salazar LGL. Methodology for estimating the modulus of elasticity of bitumen under different aging conditions by AFM. Road Mater Pav Des. 2019;20:S332–46.
36. Shaheen TI, Emam HE. Sono-chemical synthesis of cellulose nanocrystals from wood sawdust using Acid hydrolysis. Int J Biol Macromol. 2018;107:1599–606.
37. Abid K, Gholami R, Mutadir G. A pozzolanic based methodology to reinforce Portland cement used for CO_2 storage sites. J Nat Gas Sci Eng. 2020;73:103062.
38. Olivia M, Tambunan LM, Saputra E. Properties of palm oil fuel ash (POFA) geopolymer mortar cured at ambient temperature. 2017.
39. Jamaludin NFA, Muthusamy K, Isa NN, Md Jaafar MF, Ghazali N. Use of spent garnet in industry: a review. Mater Today: Proc Elsevier Ltd. 2021;48:728–33.
40. Muttashar HL, Ariffin MAM, Hussin MW, Bin IS. Realisation of enhanced self-compacting geopolymer concrete using spent garnet as sand replacement. Mag Concrete Res. 2018;70(11):558–69.
41. Masri KA, Jaya RP, Arshad AK, Mahmud MZH. Morphological and physical characteristic of stone mastic asphalt mixture incorporating nano silica. Open Civ Eng J. 2020;14(1):113–25.
42. Ji X, Hou Y, Zou H, Chen B, Jiang Y. Study of surface microscopic properties of asphalt based on atomic force microscopy. Constr Build Mater. 2020;242:118025.
43. Jeffry SNA, Jaya RP, Hassan NA, Yaacob H, Mirza J, Drahman SH. Effects of nanocharcoal coconut-shell ash on the physical and rheological properties of bitumen. Constr Build Mater. 2018;158:1–10.
44. Samsudin SM, Arshad AK, Ahmad J, Masri KA. Microstructure of nanosilica modified binder by atomic force microscopy. Jurnal Teknologi. 2016;78:33–44.
45. Ozdemir KD. Morphological investigation of SBS modified bitumen by innovative microscopies: AFM and CLSM. J Innov Transp. 2022;3(2):29–33.
46. Munera JC, Ossa A, Munera JC, Alvarez Lainez M. Effect of Polymer Modification on the Microstructure of Bitumen. 5th Eurasphalt & Eurobitume Congress. 2012.
47. Jeffry SNA. Performance of nanocarbon from coconut shell ash as bitumen modifier in asphalt mixture. Thesis: Universiti Teknologi Malaysia; 2019.